Engineering Structures 189 (2019) 260–271

Contents lists available at ScienceDirect

Engineering Structures

journal homepage: www.elsevier.com/locate/engstruct

Impact of corrosion on risk assessment of shear-critical and short lap-spliced bridges

Yijian Zhang[a,*], Reginald DesRoches[b], Iris Tien[a]

[a] School of Civil and Environmental Engineering, Georgia Institute of Technology, Atlanta, GA, USA
[b] Department of Civil and Environmental Engineering, Rice University, Houston, TX, USA

ARTICLE INFO

Keywords:
Bridge resilience
Deterioration
Corrosion
Shear failure
Lap splice
Pull-out failure
Failure probability
Seismic fragility
Failure modes

ABSTRACT

Increasing corrosion in aging reinforced concrete structures is increasing their vulnerability to failures. This is particularly true for bridges with low-ductility columns, including shear-critical columns and columns with short lap splices. This paper presents a methodology to assess the impact of corrosion on performance of these structures. The combined analytical and numerical modeling of shear-critical and lap-spliced columns is detailed, and outcomes are verified with previous experimental test data. Corrosion effects are accounted for through reduction of longitudinal and transverse reinforcement and bond deterioration between the steel and concrete through corrosion-induced cracking. The impact of corrosion on risk is assessed through conducting fragility analyses. Results quantify the increase in failure probabilities of these structures, measured by increasing probabilities of exceeding defined damage states, with increasing levels of corrosion. Corrosion is found to have a larger impact on increasing probabilities of exceeding more severe damage states. Twenty percent mass loss of reinforcement increases the probability of exceeding the complete damage state by up to 49% and 34% for a shear-critical and lap-spliced column, respectively. The effect is more pronounced at intermediate loading intensities, where there is uncertainty about the performance of the structure. Comparing between failure modes, bridges with columns of short lap splice are more vulnerable to collapse under the same degree of corrosion compared with shear-critical columns.

1. Introduction

As bridges age, they are increasingly vulnerable to failures. Bridge column failures in flexure exhibit ductile behavior, a failure mechanism that is better understood and more predictable. In contrast, shear failure and pull-out failure of columns are often brittle and catastrophic, presenting a difficult problem for structural engineers to predict their behavior. These effects are particularly pronounced during seismic events and for structures designed with light transverse reinforcement and short lap splices. For example, for highway bridges in California built pre-1970s, a typical column has transverse reinforcement of #4 stirrups at 12-inch spacing regardless of its dimensions or longitudinal reinforcement. It is also common to lap splice column longitudinal reinforcement above the footing, and the length of lap splice is around 20–24 times the longitudinal bar diameter [32,24,35]. As a result, these bridge column types have high probability of undergoing brittle failure modes. Fig. 1 shows examples from the literature of field observations of shear failure and pull-out failure of bridge columns in the 1971 San Fernando earthquake.

At the same time, deterioration of columns due to corrosion has become a critical problem for aging bridges, presenting not only significant costs for retrofitting, but also serious safety concerns under seismic conditions [17,8]. With more than one-fourth of bridges over 50 years old [16], column design details in these aging bridges make them vulnerable to brittle failure modes as well as further deterioration due to corrosion. Few previous studies, however, have investigated different failure modes of columns and quantified the impact of corrosion in these cases. This paper provides a methodology to account for deterioration due to corrosion in predictions of performance for low-ductility column types. The analysis enables the quantification of the impact of corrosion on risk assessment of these bridges through predicted failure probabilities for corroded structures.

The rest of the paper is organized as follows: the following two sections provide background on the impacts of corrosion on shear-critical and lap-spliced columns and the modeling details for the two failure modes. Verification of numerical models with experimental test data is provided. Next, the models are used to evaluate increased risks of corroded bridges through conducting seismic fragility assessments.

* Corresponding author.
E-mail address: zyj.albert@gatech.edu (Y. Zhang).

https://doi.org/10.1016/j.engstruct.2019.03.050
Received 26 October 2018; Received in revised form 7 February 2019; Accepted 17 March 2019

(a) (b)

Fig. 1. Bridge column with (a) shear failure and (b) pull-out failure in 1971 San Fernando earthquake [39].

The outcomes are probabilities of bridges with varying degrees of corrosion exceeding defined limit states under seismic load. Results show the impact of corrosion on risk for shear-critical and short lap-spliced bridges.

2. Shear-critical column considering corrosion effect

2.1. Background and modeling details

Both experimental research and post-earthquake data have shown that columns with widely spaced transverse reinforcement have a higher probability of failing in shear leading to collapse of the system [15]. This is characteristic of many bridges built prior to the 1970s before the importance of transverse reinforcement was understood. Given these vulnerabilities, it is important to be able to evaluate the column response and risk for these bridge designs. In this paper, a numerical modeling approach is used to assess bridge behavior and a calibrated shear spring element is adopted to capture shear failure degradation [21] for simulation in OpenSees [25]. More specifically, the shear spring element is able to monitor forces and deformation in the beam-column element. Shear degradation is triggered through reaching either a limiting lateral force or a limiting plastic-hinge rotation capacity [22].

Fig. 2 shows a numerical model for a double-curvature bridge column. Since boundary conditions of the bridge column are fixed at both the top and bottom in this selected bridge type, the inflection point approximately occurs at the mid-span of the bridge column. A middle node is added to capture the displacement demand at the mid-span. Two force-based beam-column elements are in series with a zero-length shear spring element and a bond slip element used to account for strain penetration effect, with the bond slip typically occurring along a portion of anchorage length [42]. Each force-based beam-column element possesses four gauss integration points, which allows the model to capture the spread of plasticity along the column and fiber section consisting of uniaxial constitutive models for steel and concrete.

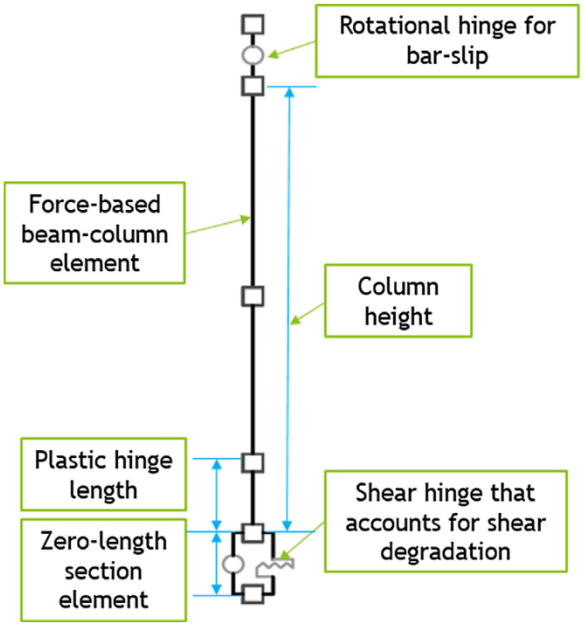

Fig. 2. Numerical model for shear-critical column.

A shear spring is added at the bottom of the column to account for the effect of shear degradation for the shear failure mode. As the shear spring element is designed for a column with rectangular cross section, the width and depth of the column are taken as $0.89D$ adopted from ACI provisions [2] and Liu et al. [23], where D is the column diameter. A detailed description of the shear spring modeling is provided in Section 2.3.

2.2. Test verification of pristine column

To verify the accuracy of the numerical model, force-displacement curves from the model are compared to those from experimental tests of circular shear-critical columns conducted by Ghee [4]. Experimental data on corroded shear-critical columns are not available, so results are compared with the pristine column. The two specimens for comparison have a diameter of 400 mm and height of 600 mm. Longitudinal reinforcement consists of 20 steel bars with a diameter of 16 mm. Transverse reinforcement consists of steel bars with a diameter of 6 mm at 60 mm and 80 mm spacing for the two specimens. Fig. 3 shows both experimental and numerical results from static cyclic tests for each specimen.

The solid line and dashed line represent experimental results and numerical results, respectively. From Fig. 3, the numerical model is able to capture the force-displacement envelope, including the point where the specimen begins to lose its load-carrying resistance due to shear failure. Table 1 shows the percentage differences in the peak force and displacement corresponding with 20% strength drop between the numerical and experimental results.

From Table 1, the percentage differences for both specimens between the experimental and numerical results are less than 5% and 10% for the peak force and displacement corresponding with 20% strength drop, respectively.

2.3. Corrosion effect on shear-critical column

Previous studies have investigated the effect of pitting corrosion on the mechanical properties of corroded steel bars [1,12,11,5]. The effects of corrosion damage on residual capacity as well as on the

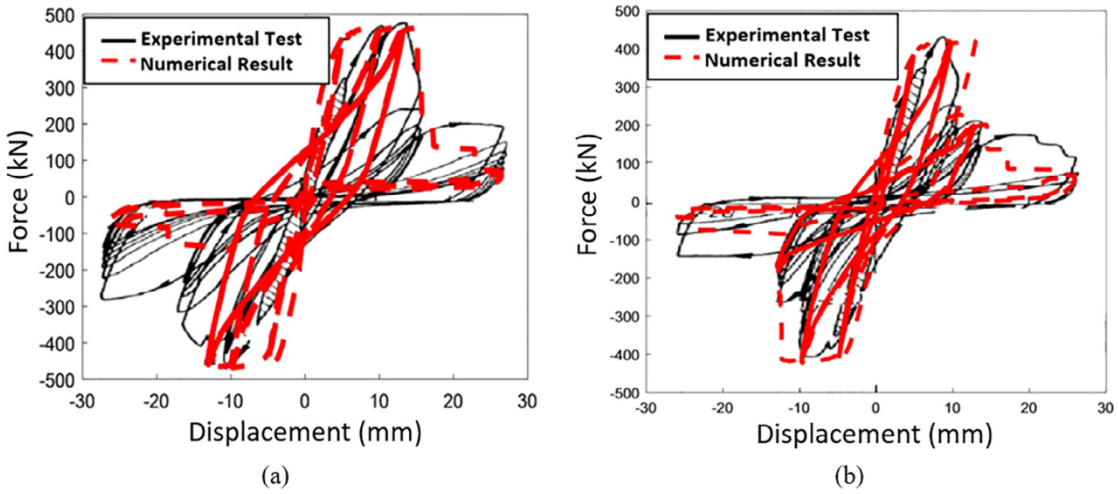

Fig. 3. Force-displacement curves for specimens with (a) 60 mm and (b) 80 mm transverse reinforcement spacing from experimental tests [4] and numerical models developed in this study.

Table 1
Comparison between experimental tests and numerical model results for shear-critical column.

	60 mm Transverse Spacing Specimen		80 mm Transverse Spacing Specimen	
	Peak Force (kN)	Displ. at 20% Strength Drop (mm)	Peak Force (kN)	Displ. at 20% Strength Drop (mm)
Experimental Test	462	15.1	468	10.1
Numerical Model	469	13.8	450	9.3
% Difference	1.6%	8.6%	3.8%	7.9%

ductility of corroded bars are adopted in this study as in Du et al. [12,11] to account for the effect of pitting corrosion on the constitutive behavior of reinforcement in tension. Kashani et al. [18] have conducted 3D optical measurements of corroded bars to investigate spatial variability in corrosion patterns, and have found that the geometrical properties of corroded bars can be modeled using a lognormal distribution. This study uses the mean values of the lognormal distribution to account for the impact of pitting corrosion on the geometric properties of corroded bars. In other words, the influence of corrosion is accounted for in terms of the averaged response of the stress-strain behavior and the averaged reduced cross section of steel with uniform mass loss [19,20].

To account for corrosion in the shear-critical column, both the strength limit curve and unloading stiffness are modified in the shear spring element. First, the strength limit curve is constructed in accordance with Eq. (1) provided in ASCE 41 [3]. The curve is then modified by considering the average reductions in diameter of reinforcement and yield strength as shown in Eq. (2) and (3).

$$V_n = k\frac{A_v f_y d_b}{s} + \lambda k\left(\frac{6\sqrt{f_c'}}{\frac{M}{VD}}\sqrt{1+\frac{N_u}{6\sqrt{f_c'}A_g}}\right)0.8A_g \tag{1}$$

$$d_{b\_cor} = \frac{d_b}{10}\sqrt{100-\psi} \tag{2}$$

$$f_{y\_cor} = f_y(1-\beta\psi) \tag{3}$$

V_n is lateral shear strength of the column and A_v is area of transverse reinforcement. d_{b_cor} and d_b are corroded and pristine diameter of either longitudinal or transverse steel bar, respectively, while f_{y_cor} and f_y are corroded and pristine yield strength of steel bar, respectively. s is spacing of transverse reinforcement, N_u is axial compression force, $\frac{M}{VD}$ is the largest ratio of moment to shear times effective depth, A_g is gross cross-sectional area of the column, and f_c' is compressive strength of concrete. λ and k are adjustment factors for displacement ductility at shear failure and lightweight concrete, respectively, and are taken to be unity in this study. $\psi/100$ is mass loss ratio and β is pitting coefficient that accounts for the influence of corrosion. Substituting Eqs. (2) and (3) into Eq. (1) and rearranging terms results in the modified strength limit as shown in Eq. (4)

$$V_{n\_cor} = C_v k\frac{A_v f_y d_b}{s} + \lambda k\left(\frac{6\sqrt{f_c'}}{\frac{M}{VD}}\sqrt{1+\frac{N_u}{6\sqrt{f_c'}A_g}}\right)0.8A_g \tag{4a}$$

$$C_v = 10(100-\psi)^{\frac{3}{2}}(1-\beta\psi) \tag{4b}$$

where C_v is the reduction factor that accounts for corrosion effect. The strength limit curve is one of the thresholds that triggers shear degradation.

Next, the unloading stiffness is modified due to corrosion. Total displacement (Δ_{total}) of the system consists of contributions from the shear spring (Δ_s) and flexural element (Δ_f). As the shear spring and flexural element are connected in series, the total unloading stiffness (K_{deg}^t) is given in Eq. (5) [15].

$$K_{deg}^t = \left(\frac{1}{K_{deg}} + \frac{1}{K_{unload}}\right)^{-1} \tag{5}$$

K_{deg} is unloading stiffness of the shear spring and K_{unload} is unloading stiffness of the flexural element. Corrosion of reinforcement has an effect on the unloading stiffness of the shear spring, and therefore, on the total unloading stiffness. The unloading stiffness of the shear spring is a function of the maximum shear strength and the residual deformation (Δ_r) [21], with residual deformation computed based on the difference in shear deformation from the shear failure point to the point of zero shear force along the backbone as shown in Eq. (6a). The residual drift ratio can be determined by column clear span (L) as in Eq. (6b).

$$\Delta_r = -\frac{|V_n|}{K_{deg}} \tag{6a}$$

$$\frac{\Delta_r}{L} = -\frac{|V_n|}{K_{deg}L} \tag{6b}$$

The relation between residual drift ratio and multiple geometric and mechanical parameters of the column is based on a stepwise regression as shown in Eq. (7).

$$\frac{\Delta_r}{L} = -0.16 - 15.4\rho_t - 0.009\frac{l_d}{d_b} + 0.7\frac{A_{cc}}{A_g} + 0.58\frac{f_y A_s}{f_c' A_g} \geq 0.02 \quad (7)$$

ρ_t is transverse reinforcement ratio, l_d is development length of longitudinal bars, A_{cc} is gross confined area bounded by transverse reinforcement in the column section, and A_s is total area of longitudinal reinforcement bars. To account for corrosion, Eqs. (6) and (7) is modified to

$$\frac{\Delta_{r\_cor}}{L} = -\frac{|V_{n\_cor}|}{K_{deg}^{cor} L} \quad (8)$$

$$\frac{\Delta_{r\_cor}}{L} = -0.16 - 15.4C_t\rho_t - 0.009C_b\frac{l_d}{d_b} + 0.7C_{cc}\frac{A_{cc}}{A_g} + 0.58C_y\frac{f_y A_s}{f_c' A_g} \geq 0.02 \quad (9)$$

where C_t, C_b, C_{cc}, and C_y are reduction factors for transverse reinforcement ratio, development ratio ($\frac{l_d}{d_b}$), confinement ratio ($\frac{A_{cc}}{A_g}$), and longitudinal steel distribution in column section ($\frac{f_y A_s}{f_c' A_g}$), respectively. Each of these corrosion reduction factors can be expressed in terms of mass loss (ψ) and pitting corrosion coefficient (β) as

$$C_t = 1 - \frac{\psi}{100} \quad (10a)$$

$$C_b = \frac{10}{\sqrt{100 - \psi}} \quad (10b)$$

$$C_{cc} = 1 \quad (10c)$$

$$C_y = 1 - \beta\psi \quad (10d)$$

Note that Eq. (10c) is unit under the assumption that corrosion has a minimal effect on the confinement ratio. From Eqs. (8) and (9), the corroded unloading stiffness of the shear spring (K_{deg}^{cor}) is expressed as shown in Eq. (11).

$$K_{deg}^{cor} = -\frac{\left| C_y k\frac{A_v f_y d_b}{s} + \lambda k\left(\frac{6\sqrt{f_c'}}{\frac{M}{VD}}\sqrt{1 + \frac{N_u}{6\sqrt{f_c'}A_g}}\right)0.8A_g \right|}{\left(-0.16 - 15.4C_t\rho_t - 0.009C_b\frac{l_d}{d_b} + 0.7C_{cc}\frac{A_{cc}}{A_g} + 0.58C_y\frac{f_y A_s}{f_c' A_g}\right)L} \quad (11)$$

Assuming corrosion has a minimal effect on the unloading stiffness of the flexural element, the updated total unloading stiffness for a shear-critical column ($K_{deg}^{t\_cor}$) is

$$K_{deg}^{t\_cor} = \left(\frac{1}{K_{deg}^{cor}} + \frac{1}{K_{unload}}\right)^{-1} \quad (12)$$

The shear spring is triggered by reaching either the strength limit or plastic hinge rotation capacity. The force-displacement relation shown in Fig. 4 is for the scenario where the strength limit is the governing factor. This scenario represents either pure shear failure in which shear degradation is triggered before yielding of longitudinal reinforcement takes place, or shear-flexure failure in which the column fails in shear with a certain level of flexural deformation. Corrosion also impacts the total unloading stiffness of the column due to change of the residual drift in the shear spring backbone curve.

Another scenario is when shear degradation is triggered when rotation of the plastic hinge region reaches its limit. Physically, this typically represents shear-flexure failure. This study assumes that corrosion has no impact on the rotational capacity across the plastic hinge at shear failure. Rotational capacity (θ_f) is computed based on Eq. (13) obtained from a stepwise regression as in Leborgne [21].

$$\theta_f = 0.027 - 0.033\frac{N_u}{A_g f_c'} - 0.01\frac{s}{d} \geq 0.006 \quad (13)$$

s is transverse reinforcement spacing and d is column depth.

The implementation of the effect of corrosion on the risk assessment of a bridge with shear-critical column is presented in Section 4. This is performed through seismic fragility assessment of a sample bridge consisting of a corroded shear-critical column. Results quantify the impact of corrosion on this failure mode in terms of increasing the probabilities of exceeding defined damage states.

3. Column with short lap splice considering corrosion effect

3.1. Background and modeling details

Many aging bridges with lap-sliced columns, including those with pre-1970s designs, include short starter bars and widely spaced transverse reinforcement in the bottom of the column. This study combines findings from several previous studies to model the behavior of lap-spliced columns. The mechanism transferring the tensile stress in the splice relies on the concrete tensile stress capacity. The concrete acts as an intermediate material that transfers forces between two adjacent bars [31]. This stress-transferring mechanism causes radially outward pressures on the concrete, leading to splitting cracks along the bars. The cracking of the concrete in tension causes initiation of softening due to degrading behavior of lap-spliced reinforcement [40]. In addition to inadequate lap-spliced length, light transverse reinforcement in the lap-spliced region reduces ductility of the column once cover concrete has spalled.

To quantify the lap-spliced constitutive behavior, this paper adopts the relations found in Priestley et al. [31] to obtain the value of maximum stress and residual stress in the splice. Eqs. (14) and (15) show maximum force and stress that can be developed in the lap-spliced region, respectively.

$$T_b = A_b f_s = F_t p l_{sp} \quad (14)$$

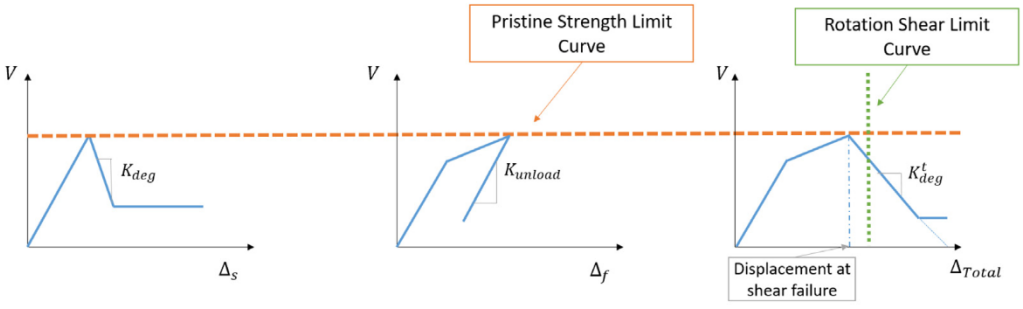

Fig. 4. Force-displacement relation and effect of corrosion with shear spring controlled by strength limit curve.

$$f_s = \frac{F_t p l_{sp}}{A_b} \tag{15}$$

T_b and f_s are force and stress developed in lap-spliced bar, respectively, A_b is cross-sectional area of longitudinal bar, F_t is tensile strength of concrete, l_{sp} is length of lap splice, and p is perimeter of cylindrical block, which is determined through Eq. (16) with an upper limit for widely spaced spliced bars.

$$p = \frac{s}{2} + 2(d_b + c) \leq 2\sqrt{2(c + d_b)} \tag{16}$$

s *is* average distance between lap-spliced bars and c is length of concrete cover. Once degradation has initiated, residual stress f_r is computed based on Eq. (17) as proposed by Wight and MacGregor [40].

$$f_r = \frac{\mu A_h f_s}{n A_b} \frac{l_{sp}}{S} \tag{17}$$

μ is frictional factor, which is taken as 1.4, A_h is cross-sectional area of transverse reinforcement, and n is number of spliced bars. This study obtains strain at both peak stress and residual stress by Tariverdio et al. [38], which assumes that displacement corresponding to maximum stress is 1 mm, and displacement corresponding to the occurrence of slip is 10 mm. Eq. (18) shows the calculation of strain at peak stress.

$$\varepsilon_s = \frac{f_s}{E_s} + \frac{\Delta_{BarSlip}}{l_{ss}} \tag{18}$$

E_s is elastic modulus of steel bar, $\Delta_{BarSlip}$ at peak stress is taken as 1 mm, and l_{ss} is the length in which displacement due to slip occurs. Fig. 5(a) shows the material constitutive behavior of lap-spliced bar [38].

Fig. 5(b) shows the numerical beam-column model that is used to capture lap-spliced failure in this study. Similar to the model for a shear-critical column, the numerical model consists of two bond-slip elements located at the top and bottom of the column as well as a middle node to account for the inflection point at the column mid-span. However, unlike the shear-critical model with two beam-column elements, this model consists of an additional beam-column element at the bottom of the column. The length of the bottom element is set to be equivalent to the length of the lap splice. Uniaxial fibers used in the bottom element constitute confined and unconfined concrete fibers as well as steel fibers with the lap-splice stress-strain model shown in Fig. 5(a), which can account for degradation triggered by lap-splice failure.

3.2. Test verification of pristine column

To verify the numerical model of the lap-spliced column, results from the model are compared with outcomes from two experimental column tests. Experimental data on corroded lap-spliced columns are not available, so results are compared with pristine columns. The first test specimen for comparison is from static cyclic tests conducted by Sun and Priestley [37]. The column has a rectangular cross section with width 730 mm and height 3.66 m. The lap splice length is 381 mm. Its longitudinal and transverse reinforcement ratios are 2.55% and 0.184%, respectively. The lap-spliced length is 20 times the diameter of the longitudinal bar. Numerical static cyclic test results (dashed line) compared to experimental results (solid line) from this specimen are shown in Fig. 6(a). The numerical model is able to predict degradation in load-carrying capacity and capture the failure mode of bond slip of lapped reinforcement.

The second test specimen is from tests conducted by Chail et al. [6]. The column is circular with a diameter of 610 mm and clear height of 3.66 m. Longitudinal and transverse reinforcement ratios are 2.53% and 0.174%, respectively. The lap-spliced length is 381 mm, which is 20 times the diameter of the longitudinal bar. Numerical compared to experimental static cyclic test results for this specimen are shown in Fig. 6(b). Comparing the numerical and experimental results, the numerical model is able to capture the degradation in load-carrying capacity as demand increases.

Table 2 shows the percentage differences between the numerical and experimental results in terms of peak force and displacement corresponding with 20% strength drop. Most of the percentage differences are below 10% except for the displacement quantity for the second specimen with around a 16% difference. This discrepancy could be caused by measurement error during the experimental test or modeling error in terms of accuracy of the fiber uniaxial behavior and damage parameters accounting for pinching behavior. However, with the other results, the numerical model is able to capture the force-displacement

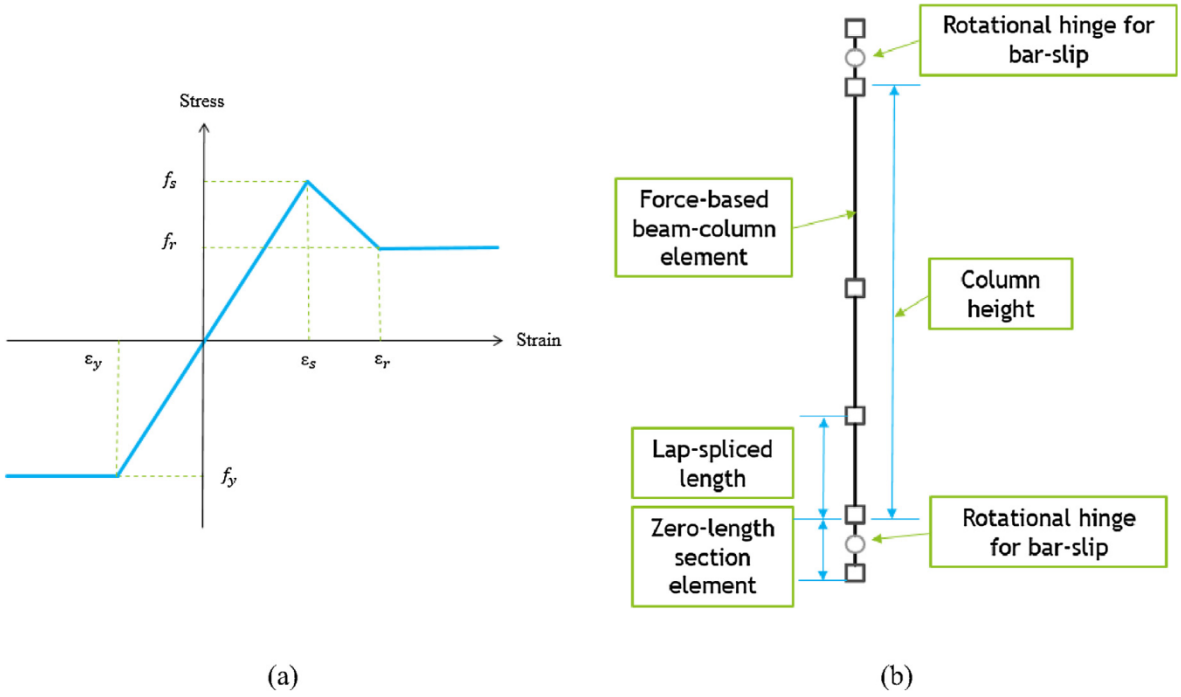

Fig. 5. (a) Constitutive material model of lap-spliced bar [38] and (b) numerical model for lap-spliced column.

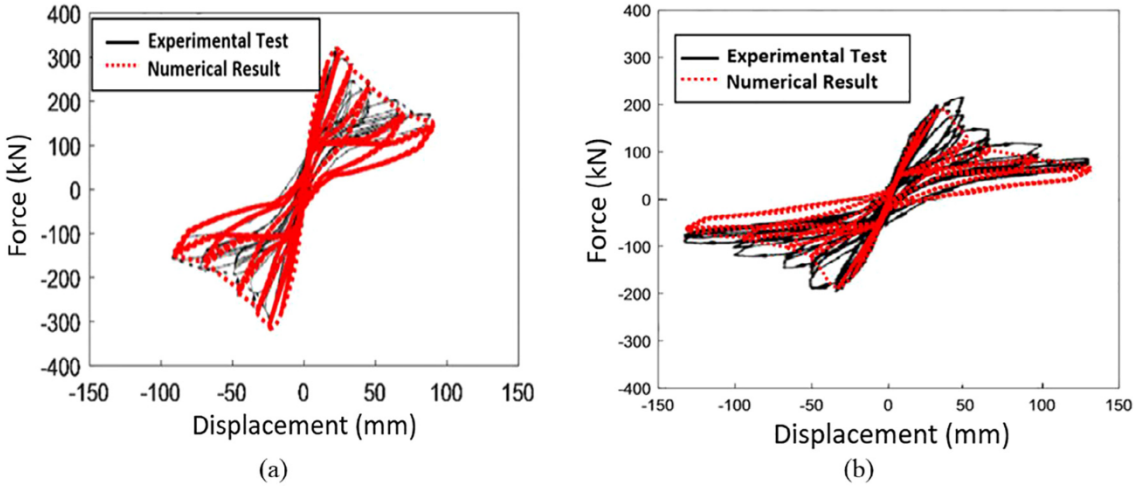

Fig. 6. Static cyclic curves comparing experimental test results from (a) Sun and Priestley [37] and (b) Chail et al. [6] with numerical results from this study.

Table 2
Comparison between experimental tests and numerical model results for lap-spliced column.

	Specimen 1		Specimen 2	
	Peak Force (kN)	Displ. at 20% Strength Drop (mm)	Peak Force (kN)	Displ. at 20% Strength Drop (mm)
Experimental Test	300	37.0	218	59.7
Numerical Model	318	39.0	198	50.1
% Difference	6.0%	5.4%	9.2%	16.2%

envelope of the lap-splice column with sufficient accuracy.

3.3. Corrosion effect on short lap-spliced column

For columns with short lap splice and wide transverse reinforcement spacing, corrosion further decreases their structural performance. Corrosion reduces the steel reinforcement section and ductility, and affects the bond between the concrete and reinforcement [33]. At the lap splice, deterioration of the bond from corrosion becomes critical, leading to bond failure. Specifically, volumetric expansion of reinforcement due to corrosion imposes tensile stress on the surrounding concrete. Micro-cracks form once the stress exceeds the tensile stress of concrete. Splitting of concrete cover due to corrosion-induced cracking leads to bond deterioration as well as loss of the force transferring mechanism described in Section 3.1.

Bond stress as shown in Eq. (19) is the bond stress that can be developed in the lap-spliced region based on an elastic cracked section analysis [36]. The ratio between the bond strength of a corroded bar and the bond strength of a non-corroded bar is expressed in terms of tensile stress and diameter of the bar as shown in Eq. (20).

$$\tau = \frac{f_s d_b}{4 l_{sp}} \tag{19}$$

$$R = \frac{\tau_{cor}}{\tau} = \frac{f_{s\_cor} d_{b\_cor}}{f_s d_b} \tag{20}$$

τ and τ_{cor} are the bond strengths of a non-corroded bar and corroded bar, respectively. Results from an empirical model based on pull-out tests of reinforced concrete specimens [13] are used to quantify the ratio R as shown in Eq. (21).

$$R = 1.0 \quad \text{for Mass Loss} \leq 1.5\% \tag{21a}$$

$$R = 1.192e^{-0.117\psi} \quad \text{for Mass Loss} > 1.5\% \tag{21b}$$

When the corrosion level is below 1.5% mass loss, R is assumed to be unity because a small amount of corrosion product increases surface roughness of the reinforcement, which actually leads to an increase in bond strength between the concrete and steel. The bond strength then decreases as mass loss increases for values above 1.5%. Substituting Eqs. (2) and (21) into Eq. (20) results in the corroded peak stress in a lap-spliced bar as shown in Eq. (22). Residual stress of the corroded lap-spliced bar, shown in Eq. (23), is derived by substituting Eqs. (2) and (3) into Eq. (17).

$$f_{s\_cor} = \frac{1}{\sqrt{1 - \frac{\psi}{100}}} f_s \quad \text{for Mass Loss} \leq 1.5\% \tag{22a}$$

$$f_{s\_cor} = \frac{1.192e^{-0.117\psi}}{\sqrt{1 - \frac{\psi}{100}}} f_s \quad \text{for Mass Loss} > 1.5\% \tag{22b}$$

$$f_{r\_cor} = \frac{(1 - 0.005\psi_t)(1 - \frac{\psi_t}{100})}{(1 - \frac{\psi}{100})} f_r \tag{23}$$

f_{s_cor} is peak stress of corroded bar, f_{r_cor} is residual stress of corroded bar, and $\psi_t/100$ denotes mass loss ratio of transverse reinforcement. Fig. 7 shows the material constitutive behavior of a lap-spliced bar for varying corrosion levels. Fig. 7(a) shows the stress-strain behavior of a spliced bar with light transverse reinforcement; for comparison, Fig. 7(b) shows the stress-strain behavior of a spliced bar with seismic transverse reinforcement design with smaller spacing assuming perfectly plastic behavior after flexural yielding of the spliced bar.

The full lap-spliced column models including corrosion are used to assess the impact of corrosion on risk for bridges subject to lap splice failures. This is done through conducting fragility assessment under varying seismic loads. Results for bridges with shear-critical and lap-spliced columns are presented in the following section. Analysis outcomes are given in terms of probabilities of exceeding damage states for each failure type considering different corrosion states.

4. Seismic fragility assessment

Before integrating the numerical models into a full bridge to perform fragility assessment, there are several steps to select the column type for the analysis starting with the material and geometric information of the column, which can influence the failure mode. Fig. 8 shows the flowchart for selecting the column type.

Note that the lap-spliced model presented in this paper is able to predict structural response of a column with both short lap splice (20–24 times d_b) and long lap splice. In other words, the lap-spliced

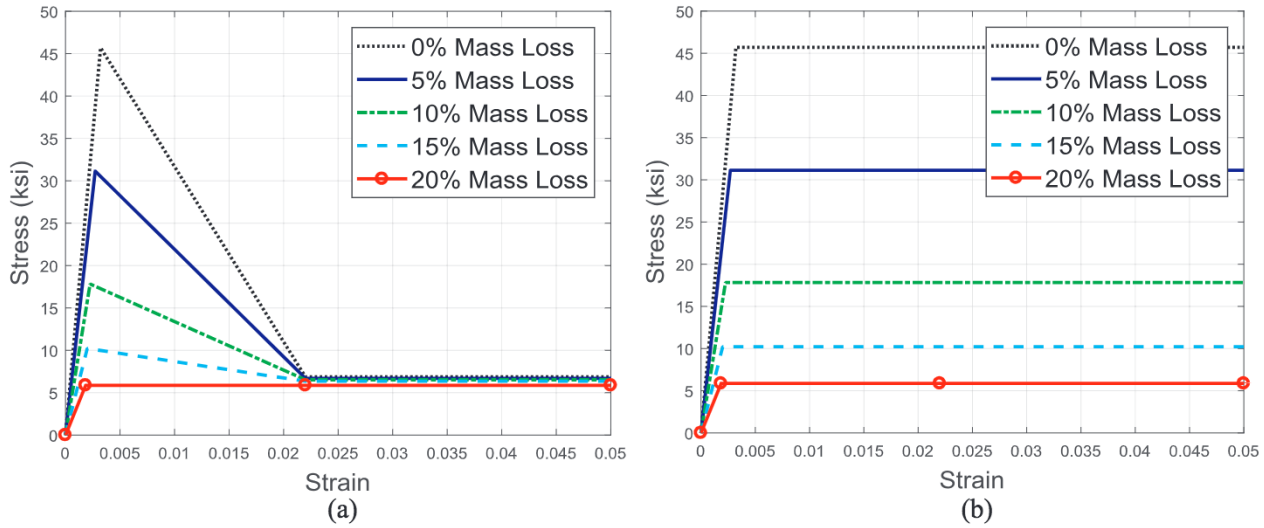

Fig. 7. Material constitutive behavior of lap-spliced bar considering corrosion effect for (a) light transverse reinforcement and (b) seismic transverse reinforcement design.

column model is able to capture both pull-out failure and flexural failure. Details of modeling the flexure-critical column are found in Zhang et al. [41]. The shear-critical column model shown in Fig. 8 is able to capture both pure shear and flexure-shear failure modes.

To assess the impact of corrosion on fragility, a full bridge is studied. The sample multi-continuous concrete single frame box girder bridge is shown in Fig. 9. This bridge type is typically used for longer spans and constitutes, for example, the bulk of the highway bridge inventory in California [32]. Table 3 summarizes the median and dispersion values of the geometric parameters describing this bridge class built before 1971. These values and the corresponding distributions are used for the generation of fragility curves in this study. Values used for column diameter are 1.2 m, 1.5 m and 1.8 m, and transverse spacing is 305 mm on center irrespective of the column size or reinforcement.

A finite-element model of this bridge is built in OpenSees. For the sub-structure, the column is modeled with fiber sections consisting of the appropriate uniaxial constitutive models for concrete and steel. This element type enables us to capture the spread of plasticity along the column. Uncertainty in material parameters include the compressive strength of concrete and yield strength of Grade 60 reinforcement. The concrete compressive strength is modeled using a normal distribution with mean 5000 psi and standard deviation 627 psi [9]. Yield strength is modeled as lognormally distributed with median 4.21 ksi and coefficient of variation 0.08 [14]. For the super-structure, it is modeled using equivalent elastic beam-column elements under the assumption that elements remain linear elastic during a seismic event. For the foundation system, translational and rotational springs are used to model pile-supported footings, which include a pile cap and piles underneath, with foundation springs consisting of zero-length elements at the base of the columns. Uncertainty in the damping of the bridge system is modeled using a normal distribution with mean 0.045 and standard deviation 0.0125 [26,29]. Further details on the modeling of bridge components can be found in Ramanathan [32].

In the fragility assessment, this study utilizes a suite of ground

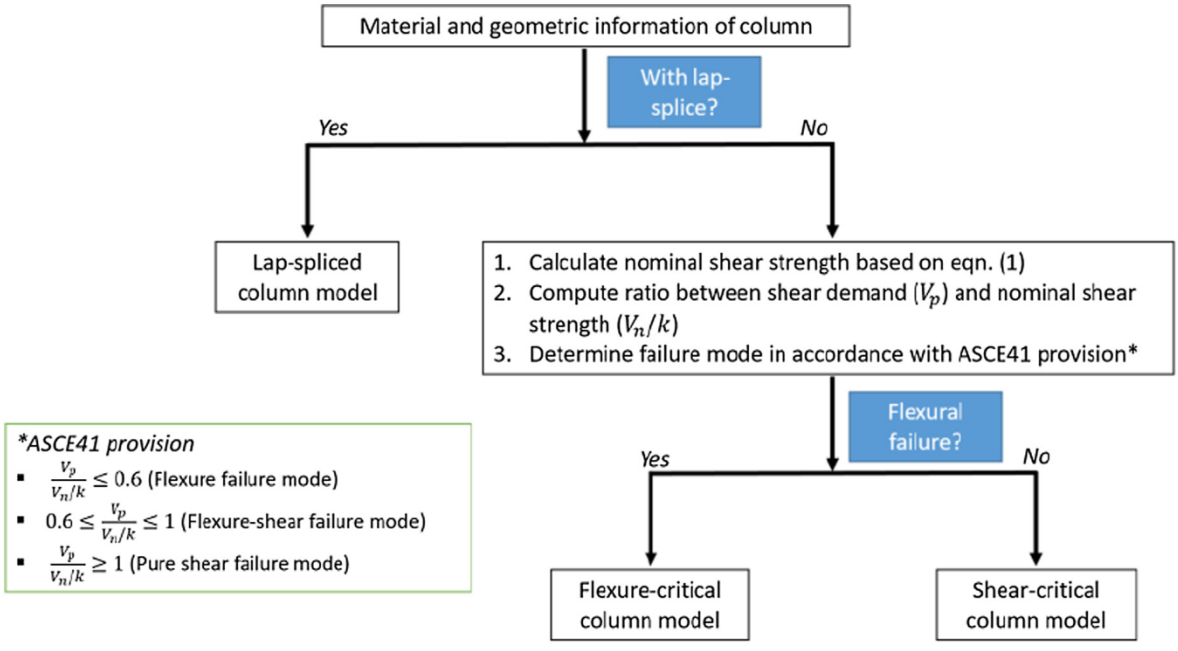

Fig. 8. Flowchart for selecting appropriate numerical model for bridge column.

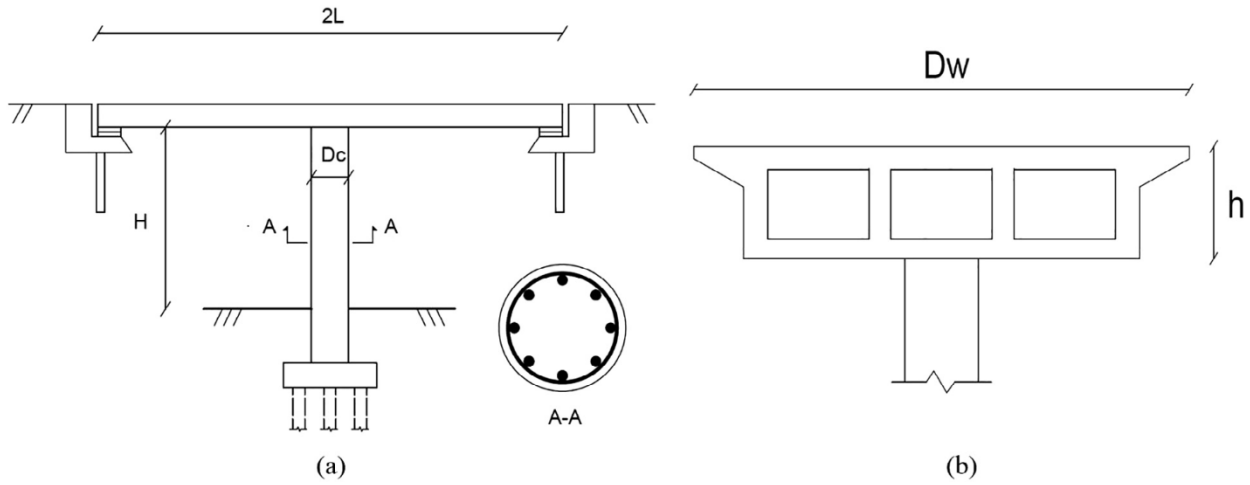

Fig. 9. (a) Longitudinal view and (b) transverse view of sample bridge.

Table 3
Median values of geometric parameters used for fragility assessment.

Geometric Parameters	Distribution Type	Median	Standard Deviation
Span length (L)	Lognormal	36.6 m	0.27 m
Deck width (Dw)	Lognormal	10.5 m	0.16 m
Column height (H)	Lognormal	6.8 m	0.12 m
Total depth of superstructure (h)	Lognormal	1.46 m	0.27 m
Longitudinal reinforcement ratio	Uniform	1.9%	0.08%

motions selected from the NGA-2 database [7]. The selected ground motion suite consists of 320 ground motions that are developed to match the hazard characteristics in California. The median response of the first 160 motions is similar to that of the full 320-motion set; therefore, the first 160 ground motions are included in the analysis. The response spectra of the ground motions in the two horizontal directions is shown in Fig. 10.

To assess risk, analytical fragility curves are computed through running a series of nonlinear time history analyses [34]. This approach is chosen to account for the multiple sources of uncertainty present in the problem, including in bridge geometries, material properties, and loading characteristics. In particular, the uncertainties considered in the analysis include the bridge geometry parameters shown in Table 3, as well as uncertainties in the top flange thickness, longitudinal reinforcement ratio, transverse reinforcement ratio, height of the abutment backwall, translational and rotational stiffness of foundation, concrete compressive strength, yield strength of reinforcing steel, gap between the girder and the shear key, gap between the deck and the abutment backwall, multiplication factor for deck mass, damping ratio, ground motions, and direction. A number of previous studies have adopted this methodology for fragility assessment [10,27,28,29,30,32]. However, these studies have not explicitly considered corrosion in shear-critical and lap-spliced columns to quantify the effect of this deterioration on predicted bridge performance.

Risk is quantified based on calculated fragilities, where fragility is defined as in Eq. (24), interpreted as the probability of exceeding a certain damage state given a specific ground motion intensity.

$$P_f = P[DS|IM = y] \tag{24}$$

P_f is probability of exceedance, DS is damage state, IM is intensity measure of ground motion, and y is realization of intensity measure. Eq. (24) can also be expressed as a function of parameters of capacity and demand variables assuming both follow lognormal distributions as shown in Eq. (25).

$$P_f = \Phi\left(\frac{\ln S_d/S_c}{\sqrt{\xi_d^2 + \xi_c^2}}\right) \tag{25}$$

S_d and S_c are the median parameters for the demand and capacity

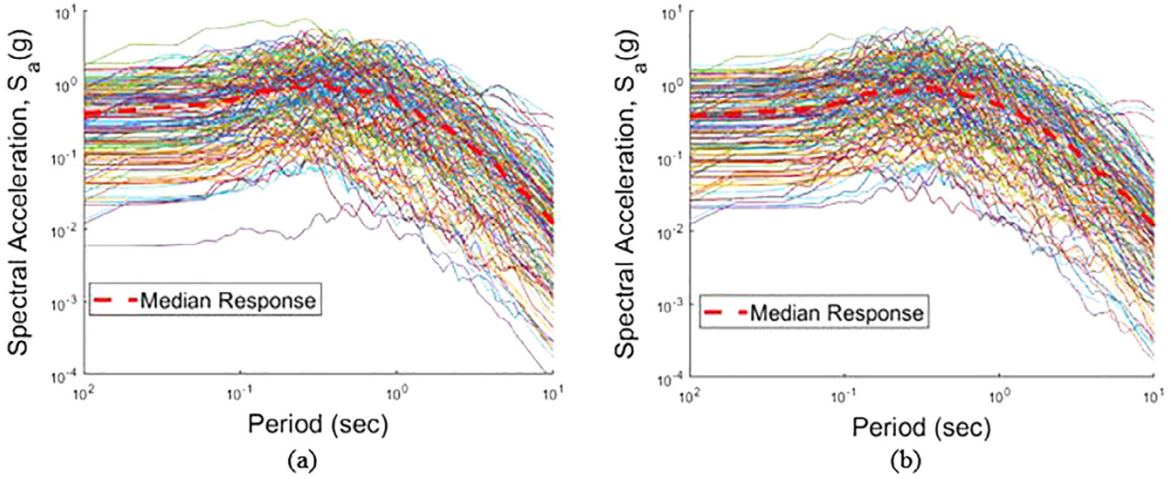

Fig. 10. Response spectra for the selected ground motions in (a) horizontal component one and (b) horizontal component two.

Table 4
Description of column damage states.

Damage State	Description	Shear-critical	Lap-spliced
DS-1	Slight	Initial cracking	Initial cracking
DS-2	Moderate	Onset of diagonal cracking	Significant cracking
DS-3	Extensive	Significant diagonal cracking	Initial spalling
DS-4	Complete	Shear failure	Complete spalling/lap-splice failure

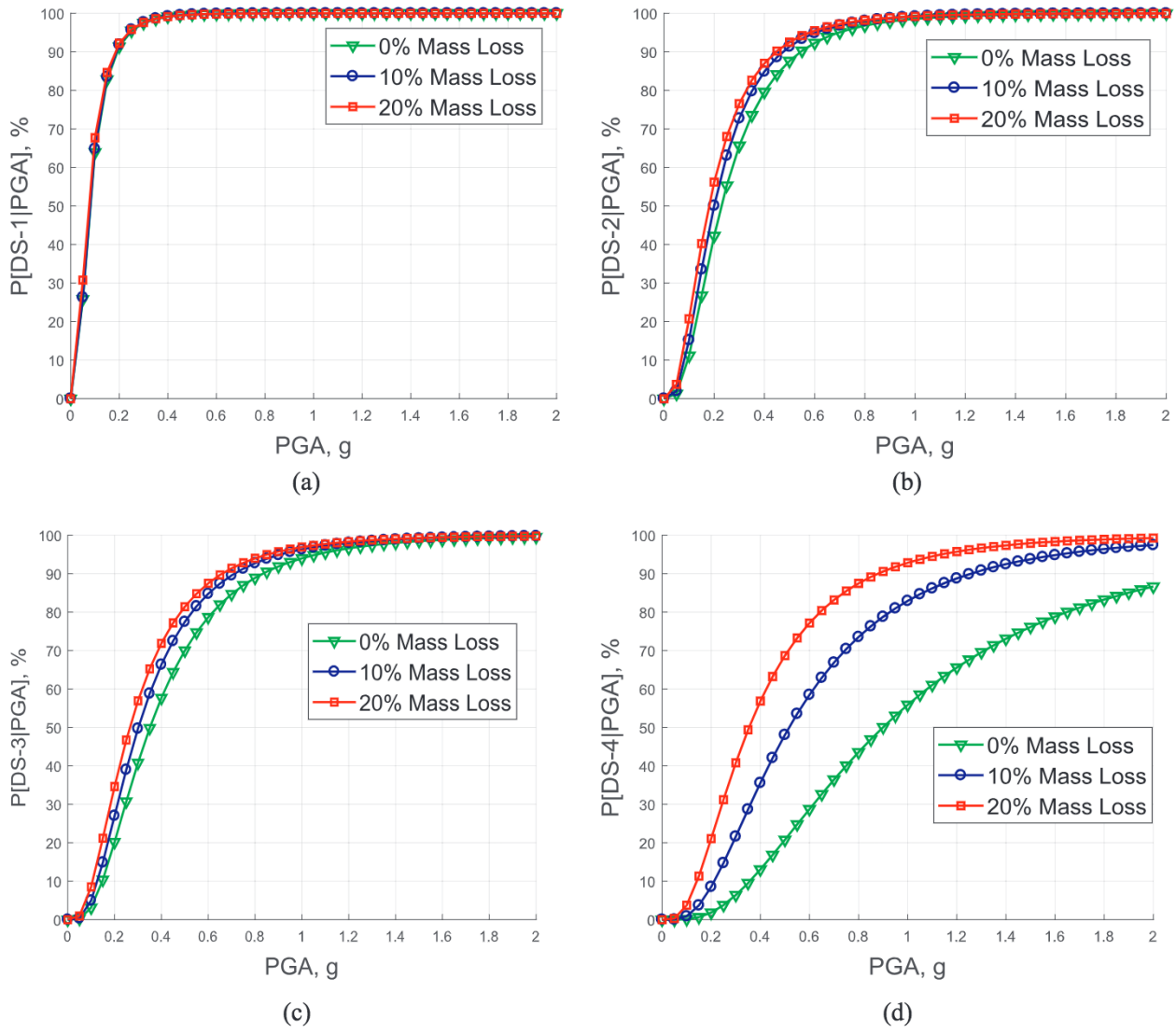

Fig. 11. Fragility curves for probabilities of exceeding (a) DS-1, (b) DS-2, (c) DS-3, and (D) DS-4 for shear-critical column with varying levels of corrosion.

distributions, respectively, ξ_d and ξ_c are the lognormal standard deviations of the demand and capacity distributions, respectively, and $\Phi(\cdot)$ is the standard normal cumulative distribution function. The engineering demand parameter used for the fragility analysis is the displacement at the mid-span of the bridge column.

Damage is discretized into four damage states as shown in Table 4. Description of each damage state for shear-critical and lap-spliced columns is provided in terms of displacement ductility. As the damage state increases, the column undergoes more damage until it reaches near collapse state (DS-4). Figs. 11 and 12 show fragility curves for shear-critical and lap-spliced columns, respectively. Fragility is given as a function of ground motion intensity as indicated by peak ground acceleration (PGA). Results provide probabilities of exceeding each damage state for columns with varying levels of corrosion as measured by percentage mass loss of reinforcement.

From Figs. 11 and 12, for both failure modes, corrosion has a minimal effect on the initial damage state. As damage accumulates, however, the influence of corrosion increases, with larger increases in the probabilities of exceeding undesired damage states compared to the non-corroded state. This is particularly seen in DS-4 (near collapse state) for shear-critical bridges. To better assess the influence of corrosion, Fig. 13 shows the difference in probability of exceeding DS-4 for each column type. The comparison is between the pristine state and the 10% mass loss and 20% mass loss corroded cases. This enables quantification of the increase in risk from corroded columns. From Fig. 13, 20% mass loss increases the failure probabilities of a shear-critical column and lap-spliced column by up to 49% and 34%, respectively. This indicates the importance of considering corrosion in assessing

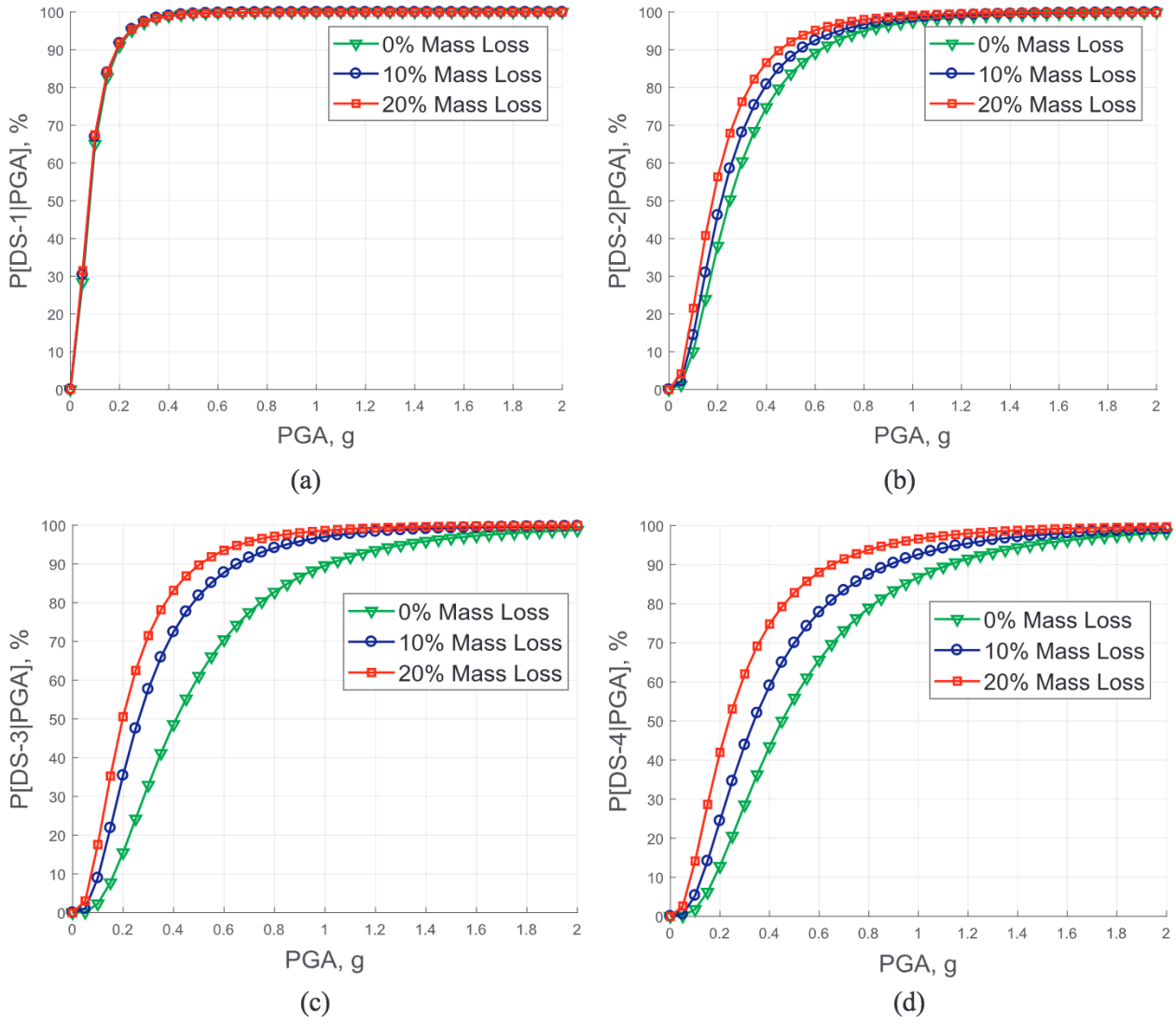

Fig. 12. Fragility curves for probabilities of exceeding (a) DS-1, (b) DS-2, (c) DS-3, and (D) DS-4 for column with short lap splice and varying levels of corrosion.

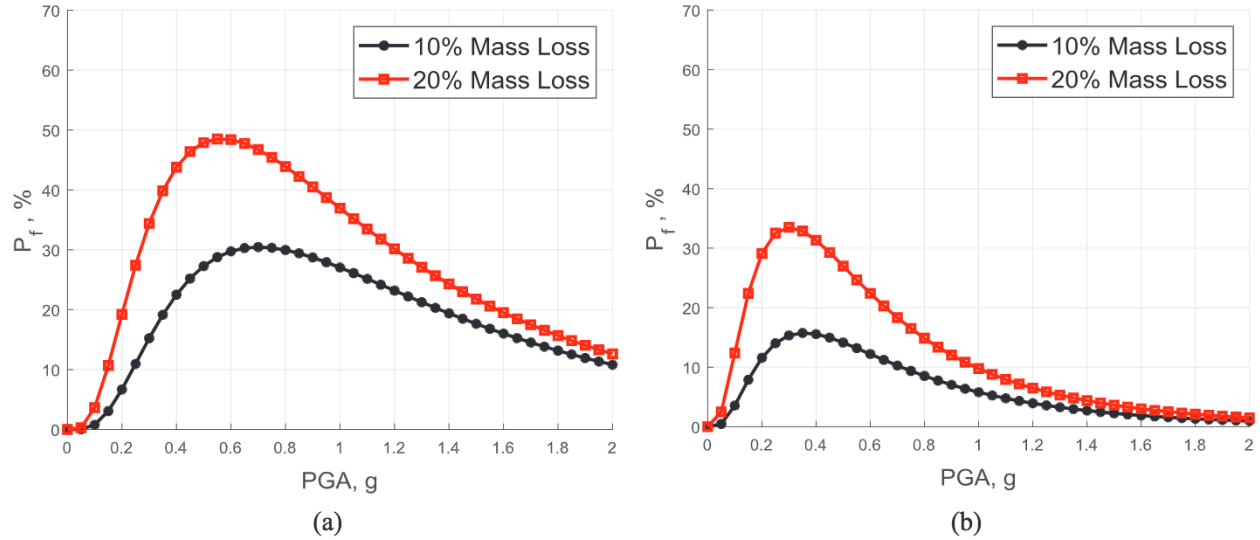

Fig. 13. Difference in failure probability for DS-4 between the pristine state and varying corrosion levels for (a) shear-critical column and (b) lap-spliced column.

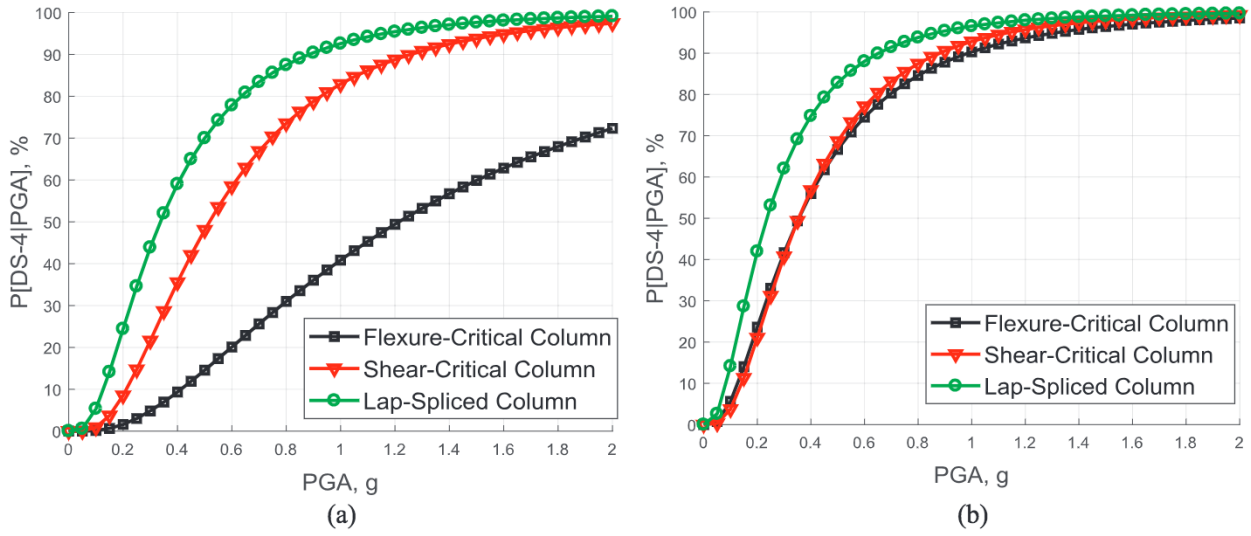

Fig. 14. Fragility curves for DS-4 considering different failure modes with corrosion levels of (a) 10% mass loss and (b) 20% mass loss.

structural risk. At higher PGA values, the effect of increasing corrosion is less pronounced. This is because under high intensity loadings, structures are more likely to fail regardless of the condition of the structure. Instead, in the intermediate loading intensities, where there is uncertainty about the performance of the structure, corrosion has a more significant effect.

To compare the effect of corrosion across failure modes, Fig. 14 shows the fragility curves for DS-4 for a shear-critical column and lap-spliced column. In addition, the authors have previously investigated the fragility of flexure-critical columns for the same bridge type. These results are also provided in Fig. 14 for comparison. The reader is referred to Zhang et al. [41] for more details on the flexure-critical analysis. From Fig. 14, lap-spliced columns are the most vulnerable at 10% mass loss, followed by shear-critical then flexure-critical columns. At 20% mass loss, lap-spliced columns remain the most vulnerable among the three. However, the difference between the three modes is less pronounced. At relatively low corrosion levels, the effect of corrosion on shear-critical columns is larger than for flexure-critical because the shear-critical case experiences additional damage due to shear degradation. In comparison, at higher corrosion levels, the effect of additional damage due to shear degradation becomes relatively less significant compared with the pure corrosion effect on the geometric and material properties of reinforcement, leading to changes in column performance. Thus, at the higher corrosion level, the failure probability of flexure-critical columns becomes close to that of shear-critical columns.

5. Conclusion

This paper presents a methodology to account for the effect of corrosion on the predicted performance of low-ductility columns, such as shear-critical columns and columns with short lap splices. The effects of corrosion considered include reduction of the amount of longitudinal and transverse reinforcement as well as weakening of the bond strength between steel and concrete through corrosion-induced cracking.

For shear-critical columns, corrosion decreases the shear capacity with decreased contribution from the transverse reinforcement. With the reduced shear strength limit, the column undergoes early shear degradation, eventually leading to brittle shear failure. For columns with short lap splice, corrosion causes volumetric expansion of reinforcement, generating tensile stress on the surrounding concrete. Consequently, cracking of concrete cover leads to bond deterioration and loss of the force transferring mechanism between the concrete and reinforcement in the lapped region. This reduces the column load-carrying capacity, leading to pull-out failure.

With these effects accounted for, the impact of corrosion on predicted performance of bridges with shear-critical and short lap-spliced columns is analyzed. This is done though conducting analytical fragility assessments. Results quantify the increases in probabilities of the bridge exceeding given damage states with increasing levels of corrosion. The results show corrosion having a larger effect with respect to more severe damage states and at intermediate loading intensities. Twenty percent mass loss of column reinforcement increases the probability of exceeding the complete damage state by up to 49% and 34% for a shear-critical and lap-spliced column, respectively. Moreover, columns with short lap splice are more vulnerable to collapse under the same level of corrosion attack compared with shear-critical columns.

Acknowledgements

This project was partially funded by the INSPIRE University Transportation Center (UTC). Financial support for INSPIRE UTC projects is provided by the U.S. Department of Transportation, Office of the Assistant Secretary for Research and Technology (USDOT/OST-R) under Grant No. 69A3551747126 through INSPIRE University Transportation Center (http://inspire-utc.mst.edu) at Missouri University of Science and Technology. The views, opinions, findings and conclusions reflected in this publication are solely those of the authors and do not represent the official policy or position of the USDOT/OST-R, or any State or other entity.

References

[1] Almusallam AA. Effect of degree of corrosion on the properties of reinforcing steel bars. Constr Build Mater 2001;15(8):361–8.
[2] American Concrete Institute (ACI) Committee 318. Building code requirements for structural concrete (ACI 318–11) and commentary. Farmington Hills, MI: American Concrete Institute; 2011.
[3] American Society of Civil Engineers (ASCE). Seismic rehabilitation of existing buildings, ASCE/SEI 41–06. Reston, VA: American Society of Civil Engineers; 2007.
[4] Ang BG. Seismic shear strength of circular bridge piers; 1985.
[5] Apostolopoulos CA, Papadopoulos MP, Pantelakis SG. Tensile behavior of corroded reinforcing steel bars BSt 500s. Constr Build Mater 2006;20(9):782–9.
[6] Chail YH, Priestley MN, Seible F. Seismic retrofit of circular bridge columns for enhanced flexural performance. Struct J 1991;88(5):572–84.
[7] Chiou B, Darragh R, Gregor N, Silva W. NGA project strong-motion database. Earthquake Spectra 2008;24(1):23–44.
[8] Choe D, Gardoni P, Rosowsky D, Haukaas T. Seismic fragility estimates for reinforced concrete bridges subject to corrosion. Struct Saf 2009;31:275–83.
[9] Choi E. Seismic analysis and retrofit of Mid-America bridges PhD. thesis Georgia: School of Civil and Environmental Engineering, Georgia Institute of Technology; 2002.

[10] Choi E, DesRoches R, Nielson BG. Seismic fragility of typical bridges in moderate seismic zones. Eng Struct 2004;26:187–99.
[11] Du YG, Clark LA, Chan AHC. Residual capacity of corroded reinforcing bars. Mag Concr Res 2005;57(3):135–47.
[12] Du YG, Clark LA, Chan AHC. Effect of corrosion on ductility of reinforcing bars. Mag Concr Res 2005;57(7):407–19.
[13] Bhargava K, Ghosh AK, Mori Y, Ramanujam S. Corrosion-induced bond strength degradation in reinforced concrete-Analytical and empirical models. Nucl Eng Design J 2007:1140–57.
[14] Ellingwood BR, Hwang H. Probabilistic descriptions of resistance of safety-related structures in nuclear plants. Nucl Eng Des 1985;88(2):169–78.
[15] Elwood KJ. Modelling failures in existing reinforced concrete columns. Can J Civ Eng 2004;31(5):846–59.
[16] Fhwa U. National bridge inventory. US: FHWA; 2013.
[17] Ghosh J, Padgett JE. Aging considerations in the development of time-dependent seismic fragility curves. J Struct Eng 2010;136(12):1497–511.
[18] Kashani MM, Crewe AJ, Alexander NA. Use of a 3D optical measurement technique for stochastic corrosion pattern analysis of reinforcing bars subjected to accelerated corrosion. Corros Sci 2013;73:208–21.
[19] Kashani MM, Lowes LN, Crewe AJ, Alexander NA. Phenomenological hysteretic model for corroded reinforcing bars including inelastic buckling and low-cycle fatigue degradation. Comput Struct 2015;156:58–71.
[20] Kashani Mohammad M, Lowes Laura N, Crewe Adam J, Alexander Nicholas A. Computational modelling strategies for nonlinear response prediction of corroded circular RC bridge piers. Adv Mater Sci Eng 2016;2016:1–15. https://doi.org/10.1155/2016/2738265.
[21] LeBorgne MR. Modeling the post shear failure behavior of reinforced concrete columns [Doctoral dissertation]; 2012.
[22] LeBorgne MR, Ghannoum WM. Analytical element for simulating lateral-strength degradation in reinforced concrete columns and other frame members. J Struct Eng 2013;140(7):04014038.
[23] Liu KY, Witarto W, Chang KC. Composed analytical models for seismic assessment of reinforced concrete bridge columns. Earthquake Eng Struct Dyn 2015;44(2):265–81.
[24] Mangalathu Sivasubramanian Pillai S. Performance based grouping and fragility analysis of box-girder bridges in California Doctoral dissertation Georgia Institute of Technology; 2017.
[25] McKenna FT. Object-oriented finite element programming: frameworks for analysis, algorithms and parallel computing Doctoral dissertation Berkeley, CA: University of California at Berkeley; 1997.
[26] Nielson BG. Analytical fragility curves for highway bridges in moderate seismic zones PhD. Dissertation Atlanta, GA: Georgia Institute of Technology; 2005.
[27] Nielson BG, DesRoches R. Seismic fragility curves for typical highway bridge classes in the Central and Southeastern United States. Earthquake Spectra 2007;23:615–33.
[28] Nielson BG, DesRoches R. Seismic fragility methodology for highway bridges using a component level approach. Earthquake Eng Struct Dyn 2007;36:823–39.
[29] Padgett JE. Seismic vulnerability assessment of retrofitted bridges using probabilistic methods PhD. Dissertation Atlanta, GA: Georgia Institute of Technology; 2007.
[30] Pan Y, Agrawal AK, Ghosn M, Alampalli S. Seismic fragility of multi-span simply supported steel highway bridges in New York State. I: bridge modeling, parametric analysis, and retrofit design. ASCE J Bridge Eng 2010;15:448–61.
[31] Priestley MN, Seible F, Calvi GM, Calvi GM. Seismic design and retrofit of bridges. John Wiley & Sons; 1996.
[32] Ramanathan KN. Next generation seismic fragility curves for California bridges incorporating the evolution in seismic design philosophy Doctoral dissertation Georgia: Institute of Technology); 2012.
[33] Rudriguez J, Ortega L, Izquierdo D, Andrade C. Calculation of structural degradation due to corrosion of reinforcements. Measuring, monitoring and modeling concrete properties. Springer; 2006. p. 527–36.
[34] Shinozuka M, Feng MQ, Kim H-K, Kim S-H. Nonlinear static procedure for fragility curve development. ASCE J Eng Mech 2000;126:1287–96.
[35] Soleimani F. Fragility of California bridges-development of modification factors Doctoral dissertation Georgia: Institute of Technology); 2017.
[36] Sotoud S, Aboutaha RS. Flexural strength of corroded lap spliced RC bridge column section. Structures congress 2014. 2014. p. 303–12.
[37] Sun Z, Priestley MJN, Seible F. Diagnostics and retrofit of rectangular bridge columns for seismic loads. San Diego: Department of Applied Mechanics & Engineering Sciences, University of California; 1993.
[38] Tariverdilou S, Farjadi A, Barkhourdari M. Fragility curves for reinforced concrete frames with lap-spliced columns; 2009.
[39] Veletzos M, Restrepo JI, Sahs S. Post seismic inspection and capacity assessment of reinforced concrete bridge columns. In: Fifth National Seismic Conference on Bridges & HighwaysMultidisciplinary Center for Earthquake Engineering Research California Department of Transportation Federal Highway Administration Transportation Research Board (No. A25).
[40] Wight JK, MacGregor JG. Reinforced concrete: mechanics and design. 5th ed. New Jersey: Prentice Hall Upper Saddle River, NJ; 2009.
[41] Zhang Y, DesRoches R, Tien I. Updating bridge resilience assessment considering corrosion inspection data. In: ASCE Engineering Mechanics Institute Conference (EMI), Cambridge, MA, May 29–June 1; 2018.
[42] Zhao J, Sritharan S. Modeling of strain penetration effects in fiber-based analysis of reinforced concrete structures. ACI Struct J 2007;104(2):133.